JOURNAL OF GEOPHYSICAL RESEARCH, VOL. 114, XXXXXX, doi:10.1029/2008JC005258, 2009

An assessment of the seasonal mixed layer salinity budget in the Southern Ocean

Shenfu Dong,[1] Silvia L. Garzoli,[2] and Molly Baringer[2]

Received 23 December 2008; revised 10 August 2009; accepted 1 September 2009; published XX Month 2009.

[1] The seasonal cycle of mixed layer salinity and its causes in the Southern Ocean are examined by combining remotely sensed and in situ observations. The domain-averaged terms of oceanic advection, diffusion, entrainment, and air-sea freshwater flux (evaporation minus precipitation) are largely consistent with the seasonal evolution of mixed layer salinity, which increases from March to October and decreases from November to February. This seasonal cycle is largely attributed to oceanic advection and entrainment; air-sea freshwater flux plays only a minimal role. Both oceanic advection-diffusion and the freshwater flux are negative throughout the year, i.e., reduce mixed layer salinity, while entrainment is positive year-round, reaching its maximum in May. The advection-diffusion term is dominated by Ekman advection. Although the spatial structure of the air-sea freshwater flux and oceanic processes are similar for the steady state, the magnitude of the freshwater flux is relatively small when compared to that of the oceanic processes. The spatial structure of the salinity tendency for each month is also well captured by the sum of the contributions from the air-sea freshwater flux, advection-diffusion, and entrainment processes. However, substantial imbalances in the salinity budget exist locally, particularly for regions with strong eddy kinetic energy and sparse in situ measurements. Sensitivity tests suggest that a proper representation of the mixed layer depth, a better freshwater flux product, and an improved surface salinity field are all important for closing the mixed layer salinity budget in the Southern Ocean.

Citation: Dong, S., S. L. Garzoli, and M. Baringer (2009), An assessment of the seasonal mixed layer salinity budget in the Southern Ocean, *J. Geophys. Res.*, *114*, XXXXXX, doi:10.1029/2008JC005258.

1. Introduction

[2] Temperature inversions in the upper water column where the surface layer is colder than the subsurface layer are common in the Southern Ocean [e.g., *de Boyer Montegut et al.*, 2007; *Dong et al.*, 2007], suggesting that salinity plays an important role in stabilizing the water column. To illustrate the importance of salinity in the Southern Ocean, we examined the contributions of temperature and salinity to the density seasonal cycle in the mixed layer. A monthly mixed layer temperature/salinity climatology was constructed from Argo float profiles (described in section 2) to compute density, and only regions with data for all months were included. The salinity contributions (ρ_s) were calculated using the time-mean temperature and monthly salinity fields, whereas the temperature contributions (ρ_t) were calculated using the monthly temperature and time-mean salinity fields.

[3] Figure 1 shows the ratio between the amplitudes of the seasonal variations in ρ_s and ρ_t, $A(\rho_s)/A(\rho_t)$, where $A(\rho_s)$ and $A(\rho_t)$ are the amplitudes of the seasonal harmonic of ρ_s and ρ_t, respectively, which suggests that the seasonal variations in the mixed layer density are generally dominated by temperature changes (ratios less than 1). However, salinity plays an increasingly important role farther south (particularly near the sea ice edge where seasonal migrations of the ice edge play a large role in determining the seasonal mixed layer density) and at other specific geographical regions. The ratio (Figure 1) exceeds 0.5 in most regions south of 40°S, particularly for regions in close proximity to sea ice and within a 5° latitude band north of the Subantarctic Front (SAF) where Subantarctic Mode Water (SAMW) is formed. This suggests that salinity contributions to the seasonal variations in the mixed layer density are about half of or nearly equal to the contributions from temperature. Therefore, the role of salinity cannot be neglected, and understanding salinity variability and what controls it are important to understanding SAMW formation, which has been linked to the upper limb of the meridional overturning circulation [e.g., *Sloyan and Rintoul*, 2001; *Rintoul and England*, 2002].

[4] Other efforts that have examined the role of salinity in the ocean have shown that salinity plays an important role in the dynamic height variability of the tropics [*Maes*, 1998; *Maes et al.*, 2002]. *Antonov et al.* [2002] examined the steric sea level variations for 1957–1994 and suggested that in the subpolar North Atlantic the contributions of temperature and salinity to the total steric sea level were nearly equal but of opposite sign. The sparseness of data in the

[1] CIMAS, RSMAS, University of Miami, Miami, Florida, USA.
[2] NOAA, AOML, Miami, Florida, USA.

0148-0227/09/2008JC005258$09.00

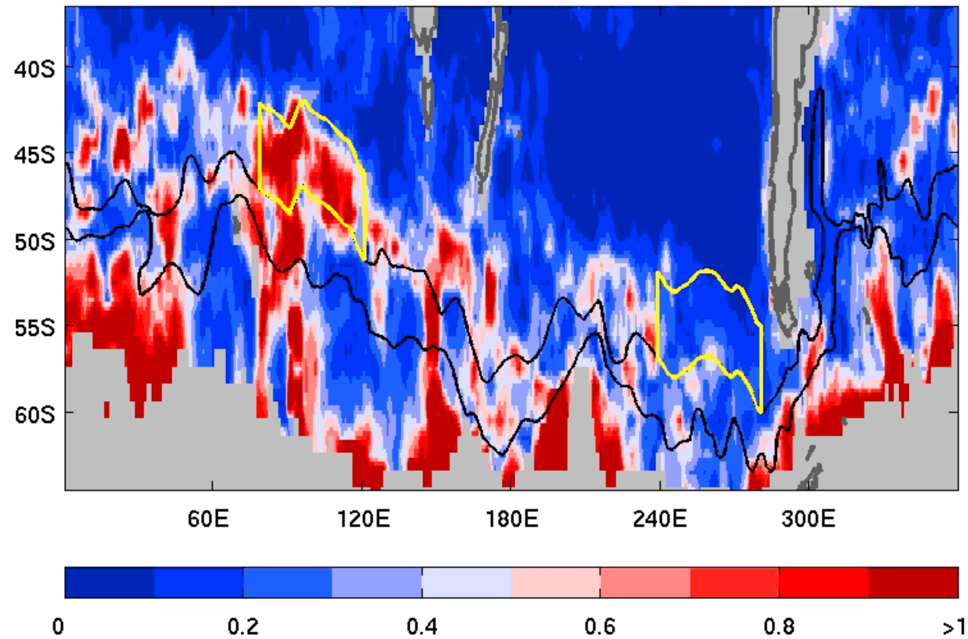

Figure 1. The ratio between the seasonal cycle amplitudes (A) of the mixed layer density due to the salinity and temperature seasonal changes, i.e., $A(\rho_s)/A(\rho_t)$. The black lines denote the Subantarctic Front (SAF, northern line) and Antarctic Polar Front (PF, southern line), respectively. The two yellow outlines indicate the areas of the regional salinity budget in the Indian and Pacific oceans.

Southern Ocean has hampered examination of the role of salinity in sea level variations. However, in view of its role in density on a seasonal time scale, we expect that salinity may play an important role in steric sea level changes in the Southern Ocean.

[5] In contrast to the extensive studies conducted on the upper ocean heat budget [e.g., *Vivier et al.*, 2002; *Dong and Kelly*, 2004; *Roemmich et al.*, 2005; *Dong et al.*, 2007], much less attention has been paid to salinity variability, again in large part due to the sparseness of available observations. Even the role of the different processes that impact seasonal salinity variability are still unknown. Previous efforts that examined the salinity balance have focused mainly on the tropics [*Cronin and McPhaden*, 1998; *Johnson et al.*, 2002; *Foltz et al.*, 2004; *Foltz and McPhaden*, 2008]. For example, the recent study by *Foltz and McPhaden* [2008] for the tropical North Atlantic discussed the complexity of the seasonal salinity balance in this region and the need for continuous in situ measurements of salinity. The lack of available observations has also limited the scope of numerous studies on salinity variability to a focus on long-term trends using measurements separated by years and decades [e.g., *Wong et al.*, 1999; *Curry et al.*, 2003; *Boyer et al.*, 2005].

[6] Up to the present, the salinity balance in the Southern Ocean has not been examined to our knowledge. Although direct observations in the Southern Ocean have historically been sparse, particularly of salinity, recent satellite and in situ observations provide some of the necessary data for a preliminary examination of the mixed layer salinity balance. Argo profiling floats provide salinity measurements with good spatial and temporal coverage. Satellite measurements of wind and sea surface height (SSH) can be used to estimate ocean Ekman and geostrophic advection, respectively, and their role in the salinity budget. Similar to air-sea heat fluxes, freshwater fluxes (evaporation minus precipitation) have large uncertainties in the Southern Ocean because of the limited available in situ data. As an example, Figure 2 shows the long-term mean freshwater fluxes obtained from the European Centre for Medium-Range Weather Forecasts (ECMWF) reanalysis 40 data and the Southampton Oceanography Centre (SOC). Although the large-scale spatial structure for both products has a positive freshwater flux (positive flux defined as out of the ocean) north of 45°S and a negative freshwater flux to the south, their detailed structure and magnitude differ substantially. With typical values of 1.5 m yr^{-1} for the long-term mean, their magnitudes can differ by 1 m yr^{-1} (Figure 2c). Thus, we must determine whether the existing data provide adequate information to close the mixed layer salinity balance.

[7] In this study, we use remotely sensed and in situ observations to evaluate whether the salinity budget of the mixed layer closes on a seasonal timescale in the Southern Ocean. To the extent that the budget does not close, what improvements can be made to the ocean observing system? Issues such as the relative role of air-sea freshwater fluxes and oceanic processes in the salinity balance, and the relative importance of horizontal advection versus vertical entrainment in the Southern Ocean, will be addressed. The upcoming 2010 salinity mission from space will stimulate numerous studies which should benefit from the present study.

[8] Section 2 provides a simplified description of the processes governing mixed layer salinity variability,

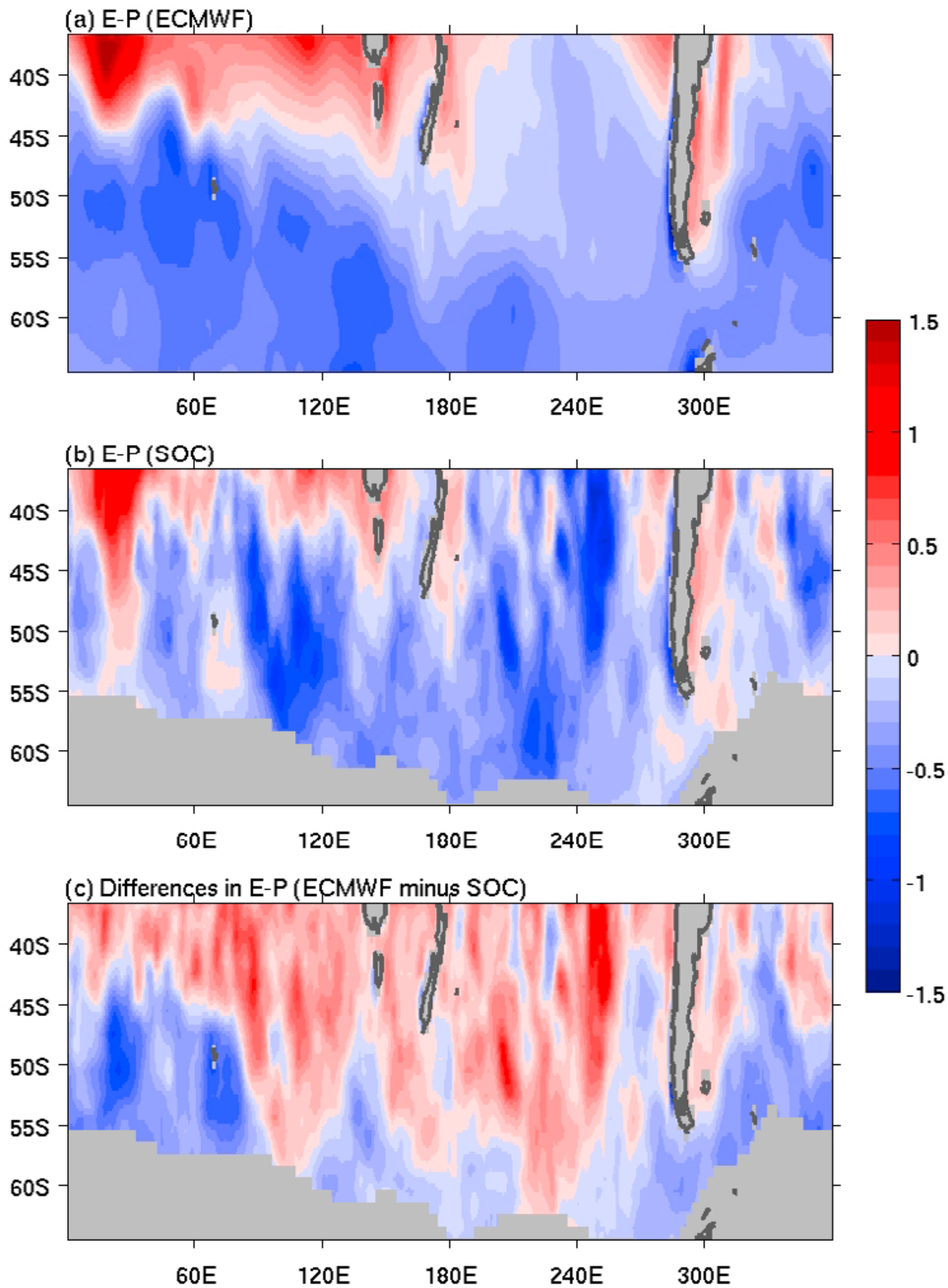

Figure 2. Long-term mean freshwater water fluxes ($E - P$) from the (a) ECMWF and (b) SOC, and (c) the differences in the long-term mean freshwater water fluxes between ECMWF and SOC. $E - P$ is defined as positive out of the ocean, i.e., increasing salinity. The units are m yr^{-1}.

followed by a discussion of the satellite and in situ observations used in this study. Section 3 describes the analyzed results of the mixed layer salinity balance. Conclusions are given in section 4. The sensitivity of the salinity budget to the choice of various data sets is given in Appendix A.

2. Method and Data

2.1. Methodology

[9] The processes governing mixed layer salinity variability are similar to those governing mixed layer temperature variability, including freshwater fluxes, horizontal advective and diffusive processes, and vertical entrainment at the base of the mixed layer. The equation for the mixed layer salinity tendency ($\partial S_m/\partial t$) is

$$\frac{\partial S_m}{\partial t} = \frac{S_m(E-P)}{h_m} - u_m \cdot \nabla S_m + \kappa \nabla^2 S_m - \frac{w_e \Delta S}{h_m}, \qquad (1)$$

where S_m is the mixed layer salinity, h_m is the mixed layer depth, w_e is the entrainment velocity, ΔS is the salinity difference between the mixed layer and just below the mixed layer, and κ is the eddy diffusivity (set to be 500 m^2 s^{-1}). The choice of eddy diffusivity does not influence the results: 500 m^2 s^{-1} is chosen simply because it provides the

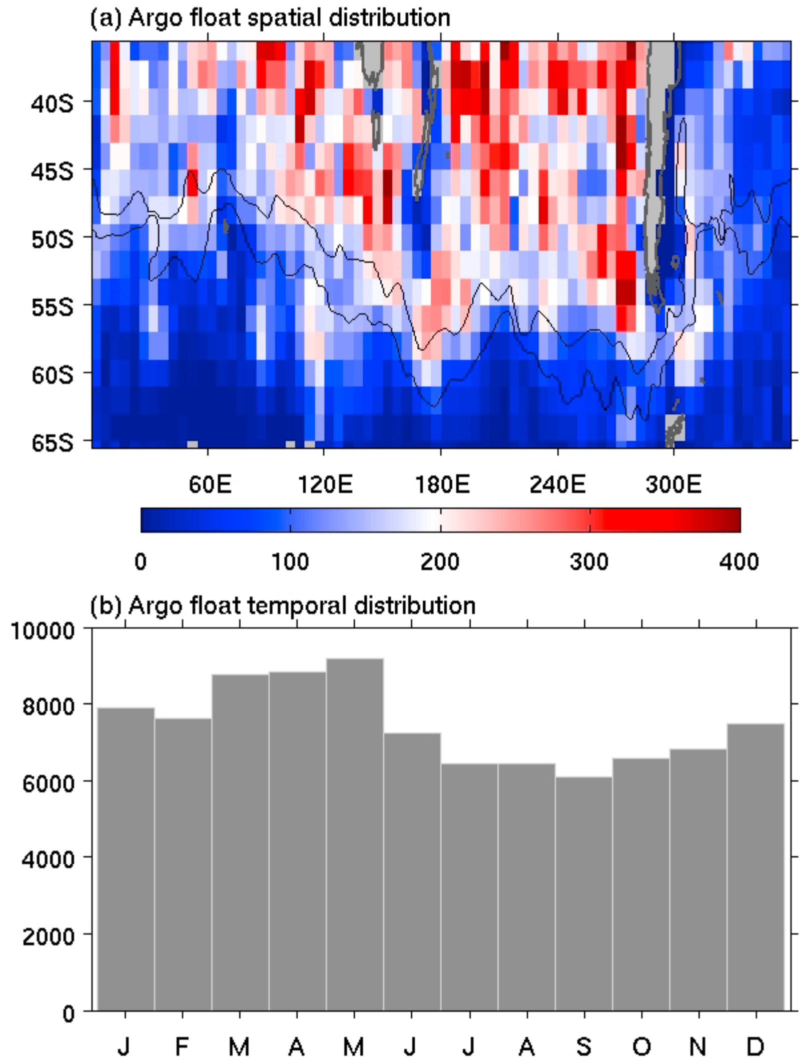

Figure 3. Number of Argo profiles (a) in each 2° latitude by 5° longitude box and (b) in each month.

minimum imbalance in the salinity budget. E and P represent the evaporation and precipitation rates, respectively, while $E - P$ is defined as positive out of the ocean and vice versa. The horizontal velocity, u_m, includes the geostrophic (u_g) and Ekman (u_e) components. All terms in (1) were directly estimated from in situ and satellite observations. Freshwater fluxes from river runoff and ice melt were not included due, in large part, to the sparsity of data available to account for them explicitly. Instead, the residual imbalance includes these processes.

2.2. Data

[10] Gridded fields for both S_m and h_m were derived from Argo float profiles of temperature, salinity, and pressure [*Gould and the Argo Steering Team*, 2004]. All available Argo profiles south of 30°S with a "good" quality flag from January 2000 to June 2008 were used, while profiles with pressure offset errors were excluded (http://www.usgodae.org/argo/news/). The number of profiles in each 2° latitude by 5° longitude grid box (Figure 3a) indicated that there were more profiles in the Pacific and Indian oceans to the north of the SAF. The number of profiles in each month (Figure 3b) varied from 7000 in September to 9000 in May with little seasonal bias. Following *de Boyer Montegut et al.* [2004] and *Dong et al.* [2008], we determined the mixed layer depth, h_m, from individual float profiles based on a density difference criterion, $\Delta\rho$ = 0.03 kg m^{-3}, where $\Delta\rho$ is the density difference from the topmost near-surface value. A monthly climatology was then objectively mapped [*Roemmich*, 1983] from the individual h_m using a decorrelation scale of 2° latitude by 5° longitude and 30 days in time. A detailed description of the mixed layer depth in the Southern Ocean is given by *Dong et al.* [2008]. Using the same objective analysis as *Dong et al.* [2008], a monthly climatological salinity map was derived from individual Argo salinity profiles.

[11] The net freshwater flux, $E - P$, includes two components, evaporation (E) and precipitation (P), and a number of E and P products are available. A monthly climatology constructed from 12 years (1990–2001) of ECMWF reanalysis 40 data (ERA40) [*Uppala et al.*, 2005] was used in this study because it provided the best balance in terms of root-mean-square (RMS) differences between the salinity tendency and the sum of the contributions from the freshwater flux, ocean advection-diffusion, and entrainment processes. The ERA40 freshwater fluxes are on a 2.5° × 2.5° grid, which were linearly interpolated

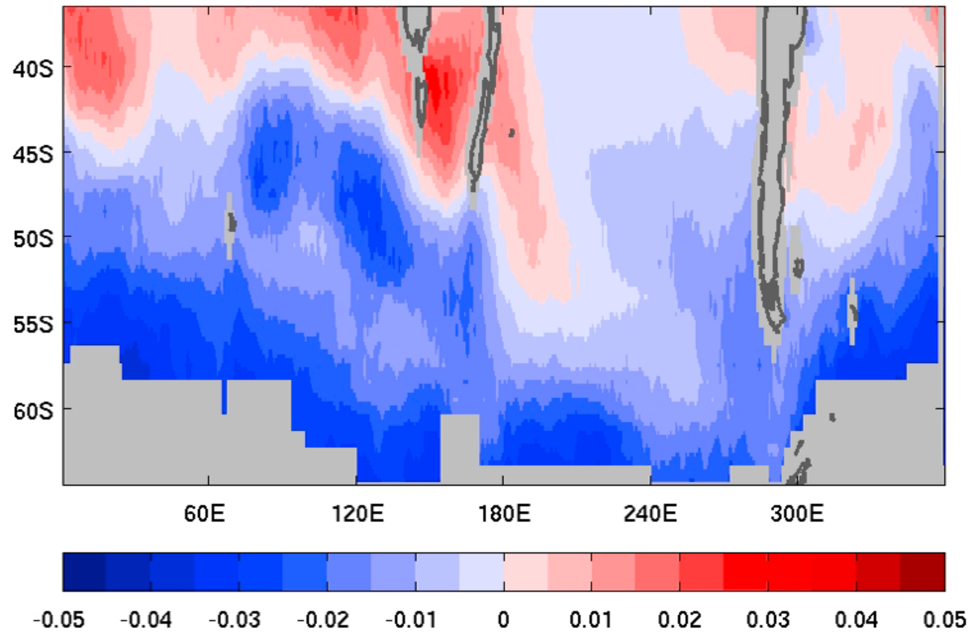

Figure 4. The time-mean salinity difference (psu) between the mixed layer and just below the mixed layer from Argo float profiles.

to a $1^\circ \times 1^\circ$ grid to match the salinity maps. The sensitivity of the results to the various $E - P$ products is given in Appendix A.

[12] The oceanic advection term ($u_m \cdot \nabla S_m$) includes both the geostrophic ($u_g \cdot \nabla S_m$) and the Ekman ($u_e \cdot \nabla S_m$) components. We made use of the geostrophic velocity (u_g) product produced by AVISO (Archiving, Validation and Interpretation of Satellite Oceanographic data), which is derived from the merged SSH fields of all available satellites (TOPEX/POSEIDON, Jason-1, ERS-1 and 2, Envisat, GFO). The satellite-derived geostrophic velocity fields are on a 7 day temporal resolution and a $1/3^\circ \times 1/3^\circ$ spatial resolution [*Ducet et al.*, 2000]. To be consistent with the temporal period and spatial resolution of the salinity maps derived from Argo profiles, the satellite velocity fields from January 2000 to June 2008 were averaged to produce a monthly climatology on a $1^\circ \times 1^\circ$ grid.

[13] We used pseudostress fields from the Center for Ocean-Atmospheric Prediction Studies (COAPS) to estimate the Ekman velocity, u_e, which is related to the surface wind stress (τ) by $u_e = \tau \times \hat{k}/\rho_0 f h_m$ The COAPS gridded wind fields were objectively mapped onto a $1^\circ \times 1^\circ$ grid from QuikSCAT scatterometer measurements [*Pegion et al.*, 2000]. We computed 6-hourly stress fields using the parameters of *Yelland and Taylor* [1996] for the period January 2000 to June 2008 and used the averages to produce a monthly wind stress climatology. We used h_m to represent the Ekman depth due to the lack of knowledge about the true Ekman depth in the Southern Ocean. The sensitivity of the salinity budget to this approximation is discussed in Appendix A.

[14] The last term on the right-hand side of (1) describes the entrainment of water from below the base of the mixed layer. The entrainment velocity (w_e) was determined from the turbulent kinetic energy balance, which is controlled by wind stirring and a stabilizing effect due to surface heating. A detailed description of w_e is given by *Qiu and Kelly* [1993] and *Dong and Kelly* [2004]. Turbulent heat fluxes derived from the Objectively Analyzed air-sea Fluxes (OAFlux) [*Yu and Weller*, 2007] were used to calculate w_e, as were radiation fluxes from the International Satellite Cloud Climatology Project (ISCCP) [*Zhang et al.*, 2004] and wind stress fields from COAPS. The entrainment velocity was set to zero during the detraining period. The OAFlux product integrates satellite observations with surface moorings, ship reports, and atmospheric model reanalyzed outputs. Daily and monthly turbulent OAFlux data for 1958–2006 are available on a $1^\circ \times 1^\circ$ grid. We used the monthly OAFlux data from 2000 to 2006 to derive a monthly climatology. The ISCCP radiative fluxes for 1983–2006 are available with a spatial resolution of $2.5^\circ \times 2.5^\circ$. We averaged the 3-hourly ISCCP radiative fluxes from 2000 to 2006 to produce a monthly climatology and then linearly interpolated it to a $1^\circ \times 1^\circ$ grid to match the salinity maps.

[15] The salinity differences (ΔS) between the mixed layer and just below the mixed layer were calculated from individual float profiles directly, then objectively mapped to a monthly climatology with a $1^\circ \times 1^\circ$ grid. These salinity differences are relatively stable in time. Figure 4 shows the yearly averaged ΔS. The mixed layer is generally fresher than the subsurface layer, as shown by the negative ΔS, particularly south of 45°S. The positive ΔS to the north, except in the center of the Pacific and Atlantic oceans, indicates that the mixed layer is saltier than the subsurface layer. The spatial structure of ΔS is most likely due to the spatial distribution of the air-sea freshwater flux ($E - P$), which is positive north of 40°S and negative to the south (Figure 2). Positive ΔS is also seen extending from the northwest to the southeast in the western Pacific, which is

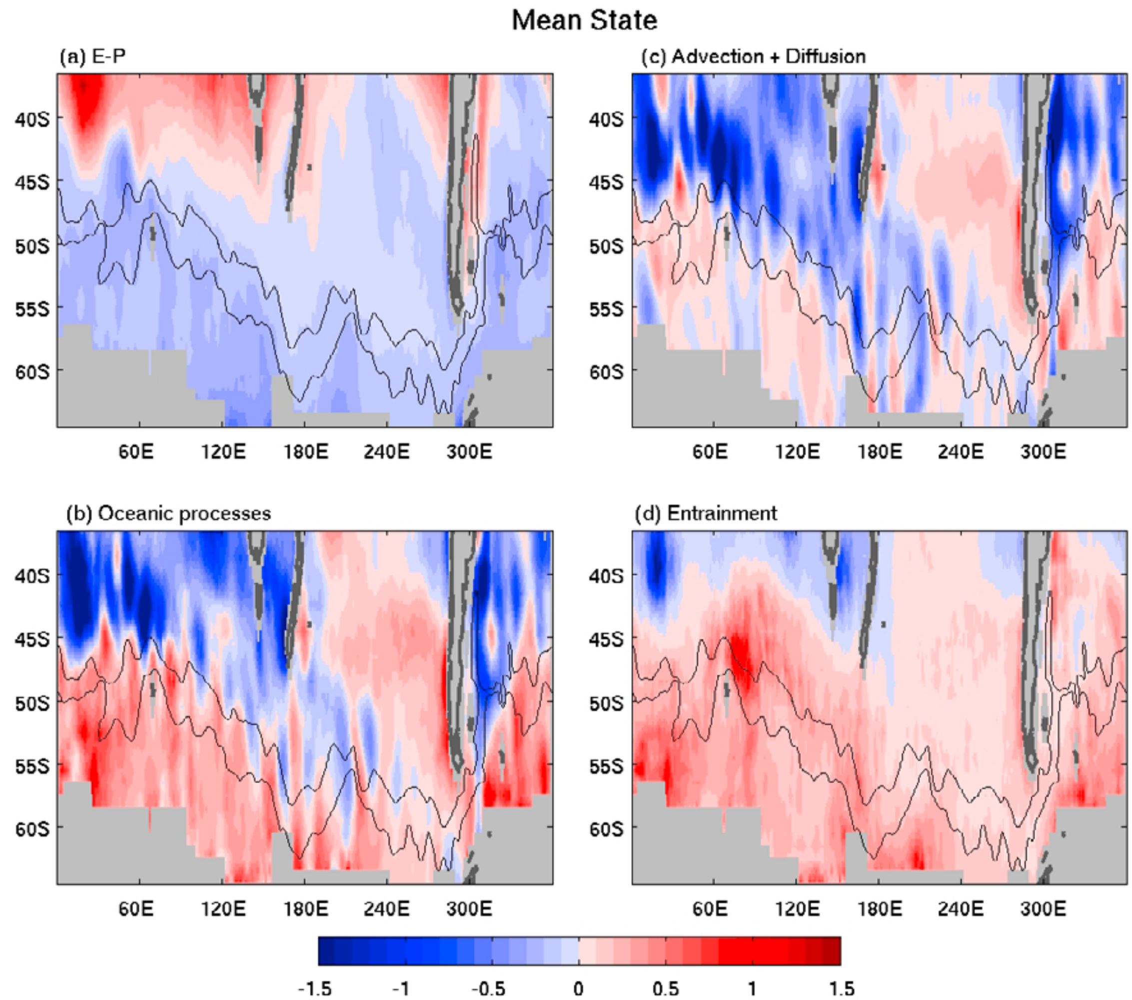

Figure 5. Spatial distribution of the time-mean (a) air-sea freshwater flux defined as positive out of the ocean ($S_m(E-P)/h_m$), (b) oceanic processes (advection + diffusion + entrainment), (c) advection-diffusion term, and (d) entrainment. The black lines denote the SAF and PF, respectively. Units are psu yr^{-1}.

probably related to the advection of the saltier water by the subtropical gyre.

[16] An autocorrelation analysis indicates that the freshwater fluxes have an e-folding scale of 8° latitude by 16° longitude, suggesting that the freshwater fluxes are potentially smoother than other variables such as the wind stress and SSH fields. To roughly match the spatial resolution of all of the variables, we smoothed the salinity and velocity fields using an 8° × 8° trianglular filter. This smoothing process effectively reduced eddy features in the geostrophic advection along the Antarctic Circumpolar Current (ACC), which do not appear in the other data sets and, subsequently, improved the balance of the mixed layer salinity budget.

3. Results

[17] We first examine the steady state to evaluate how well the contributions of freshwater flux and oceanic processes are balanced over the long-term average. We then focus on the seasonal variability of the salinity budget. We note that the results shown in this section (our base case) are our best estimate in terms of the balance between the salinity tendency (left-hand side of equation (1)) and the sum of the contributions (right-hand side of equation (1)) from the freshwater flux, ocean advection-diffusion, and entrainment processes. The sensitivity of the results to the choice of data set is given in Appendix A.

3.1. Mean State

[18] For the steady state, the freshwater flux through the air-sea interface should be balanced by the oceanic processes (advection, diffusion, and entrainment). In general, the $E-P$ is negative in our study region except to the north of 45°S in the eastern part of each ocean basin. The negative $E-P$ causes a freshening of the mixed layer. The overall spatial pattern of the $E-P$ (Figure 5a) and that of the sum of the oceanic processes (Figure 5b) are similar, but with opposite sign as expected, except in the southern part of the subtropical gyre in the Atlantic (35°S–45°S, 320°E–350°E) and to the north of the SAF in the eastern Indian and western Pacific oceans where both $E-P$ and the oceanic processes show negative values, i.e., a freshening effect to the mixed layer. However, the magnitude of the $E-P$ is smaller than that of the oceanic processes, and the small-

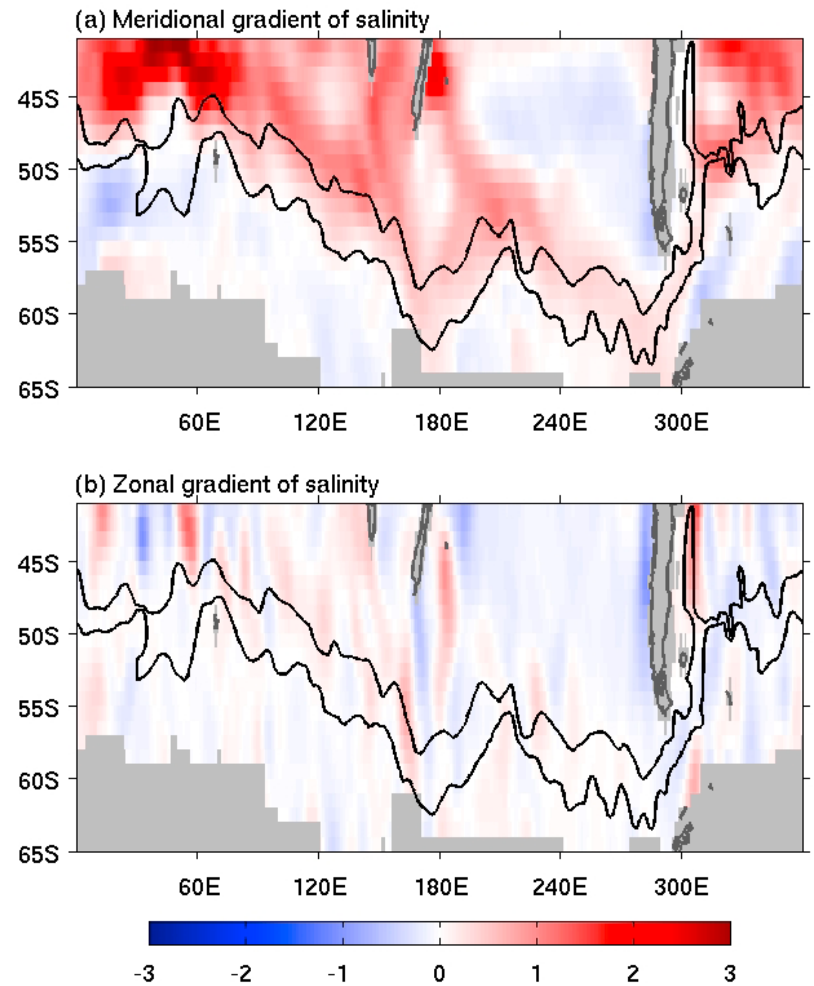

Figure 6. The (a) meridional and (b) zonal salinity gradient from the time-mean mixed layer salinity field. Units are 10^{-6} psu m^{-1}.

scale structure shown in the oceanic processes is missing from the $E - P$.

[19] Dividing the oceanic processes into horizontal (advection-diffusion) and vertical (entrainment) terms, we found that the advection-diffusion term (Figure 5c), dominated by Ekman advection, acts to reduce mixed layer salinity in the Atlantic and Indian oceans north of the ACC. To the south of the Polar Front (PF) and in the Pacific Ocean, the advection-diffusion term tends to increase the salinity. An examination of the velocity and salinity gradient fields suggests that the spatial structure of the advection-diffusion processes can be attributed to the meridional salinity gradient (Figure 6). The spatial structure of the entrainment term (Figure 5d) is very similar to that of the $E - P$ term, but of opposite sign. The entrainment is positive over most regions in the Southern Ocean except to the north of 40°S in the Indian and eastern Atlantic oceans.

[20] Although the velocity and salinity fields were smoothed to roughly match the $E - P$ decorrelation scale, a relatively small-scale structure is still shown in the oceanic processes (Figure 5b), in particular along the ACC. This small-scale feature is missing from the $E - P$ term (Figure 5a), suggesting that a better $E - P$ product could improve studies with a focus on the ACC region.

3.2. Seasonal Variations

3.2.1. Domain Average

[21] In this section we examine the salinity balance averaged over the entire Southern Ocean (0–360°E, 35°S–65°S) to evaluate how well the seasonal cycle of the mixed layer salinity is captured on a basin-wide scale by the air-sea freshwater exchange, ocean advection, diffusion, and vertical entrainment terms.

[22] As shown in Figure 7a, the sum of the contributions (gray line) to salinity change from air-sea freshwater flux, ocean advection-diffusion, and entrainment well captures the annual evolution of the salinity tendency (black line) on the domain average, although the sum of the contributions has a negative bias when compared to the salinity tendency. The salinity tendency is positive from March to October and negative from November to February, indicating that salinity in the mixed layer increases from austral fall to winter and decreases from summer to spring. The salinity tendency reaches its maximum in May and minimum in December. To examine the potential causes for the lower bias in the

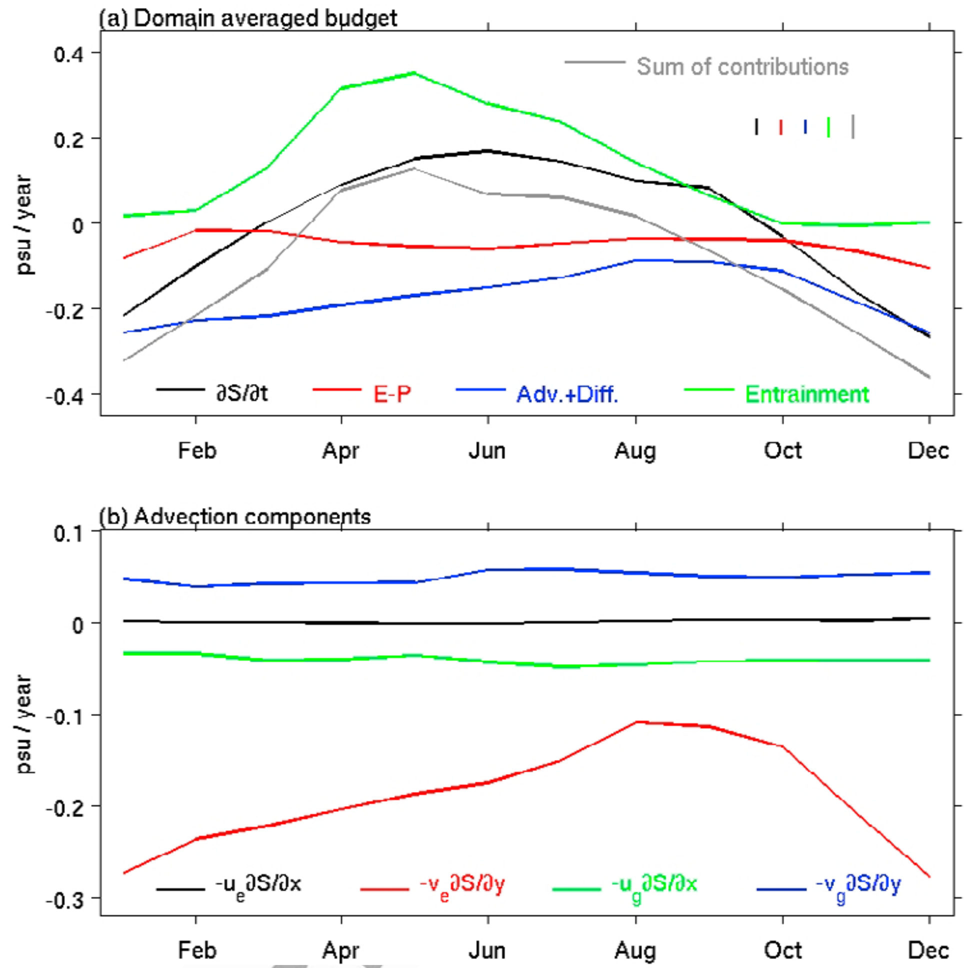

Figure 7. (a) Domain-averaged salinity budget for the Southern Ocean (35°S–65°S). The gray curve is the sum of the contributions from air-sea freshwater fluxes (red, positive out of the ocean), oceanic advection-diffusion (blue), and vertical entrainment (green) to the salinity tendency (black). (b) Contributions of the zonal and meridional geostrophic advection and Ekman advection to the total advection. The vertical lines in Figure 7a correspond to one standard error for each term. Units are psu yr^{-1}.

sum of the contributions (Figure 7), we performed an examination of the seasonal mixed layer temperature budget with temperature maps derived from the Argo profiles in a similar manner as the salinity maps. Using the same velocity and mixed layer depth fields, the sum of the air-sea heat fluxes from the OAFlux and oceanic processes roughly balances the temperature tendency, suggesting that the velocity fields are reasonable. The negative bias in the sum of the contributions (gray line, Figure 7a) is most likely due to the biases in the air-sea freshwater fluxes ($E - P$).

[23] An examination of each term on the right-hand side of (1) suggests that the seasonal cycle of the surface salinity is dominated by oceanic processes: horizontal advection-diffusion and vertical entrainment. The advection-diffusion term is always negative throughout the year, which can be attributed to the year-round westerly wind transporting fresher water from the south to the north. The advection-diffusion shows a weak seasonal cycle, with its maximum freshening effect in December and January. This maximum advective freshening effect in austral summer is probably related to the ice melting near Antarctica, which is subsequently transported to the north via the Ekman process. The domain-averaged entrainment is positive year-round and experiences a strong seasonal cycle. The entrainment reaches its maximum in May and June, then decreases to zero by August. Similar to the advection-diffusion term, the air-sea freshwater flux term is also negative year-round, but its magnitude is about half of the advection-diffusion term. Unlike the mixed layer temperature budget where the air-sea heat exchange dominates its seasonal cycle, the air-sea freshwater flux plays little role in the seasonal variability of the mixed layer salinity averaged in the Southern Ocean.

[24] By dividing the advection-diffusion term into geostrophic advection, Ekman advection, and diffusion components (not shown), similar to the mixed layer temperature budget of *Dong et al.* [2007], we found that the contribution of the geostrophic advection is negligible. The diffusion term is also very small and does not contribute to the S_m seasonal cycle on the domain average. Most of the variations in the advection-diffusion term come from the Ekman advection. We further divide the advection into zonal and meridional components (Figure 7b). The Ekman advection

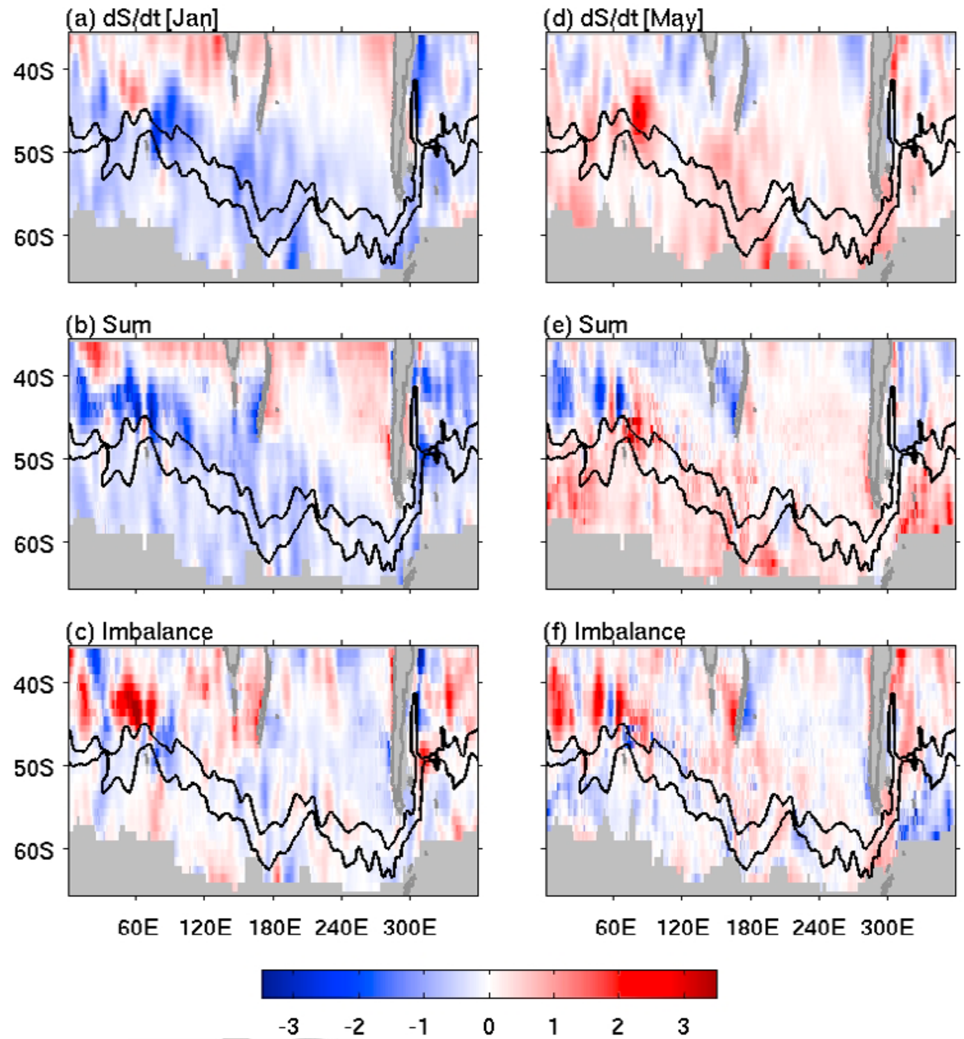

Figure 8. Spatial distribution of salinity tendency, the sum of the contributions to the salinity tendency, and their differences (salinity tendency minus the sum) for (a–c) January and (d–f) May, respectively. Units are psu yr^{-1}.

is dominated by the meridional component, whereas the zonal component is close to zero. This is consistent with the large meridional Ekman transport from strong westerly winds and a large meridional salinity gradient. Both the zonal and meridional components of the geostrophic advection are relatively small when compared to the meridional Ekman advection, but not negligible. The minimal role of geostrophic advection in the salinity tendency is due to the compensation of its zonal and meridional components (Figure 7b).

3.2.2. Spatial Variation

[25] To illustrate the spatial distribution of each term and to assess how well the atmospheric and oceanic processes capture the spatial structure of the salinity tendency, Figures 8 and 9 show all of the individual components in equation (1), their sum, and the differences between the left-hand and right-hand sides of equation (1) during January (Figures 8a–8c and 9a–9d) and May (Figures 8d–8f and 9e–9h). These components approximately correspond to the maximum and minimum of the salinity tendency.

[26] In January, the salinity tendency (Figure 8a) is negative over most regions south of 45°S and positive near the northern boundary in the Indian and Pacific oceans, except in the central Pacific. The sum of all of the contributions (Figure 8b, right-hand side of equation (1)) shows similar spatial patterns to the salinity tendency. However, its magnitude is larger than that of the salinity tendency as shown by their differences (Figure 8c). Large differences between the salinity tendency and the sum of the contributions are seen to the north of the ACC in the Atlantic and Indian oceans where the sum of the contributions shows a strong freshening effect. The surface freshwater flux term (Figure 9a) is negative south of 45°S and positive to the north, except in the center of the Pacific and Atlantic oceans. The minimum $E - P$ term occurs to the north of the ACC, where the salinity experiences strong freshening (Figure 8a). The Ekman advection (Figure 9b) is mostly negative, with the strongest freshening effect north of the ACC. Positive Ekman advection occurs in the southeast Pacific (40°S–55°S) and in the region close to

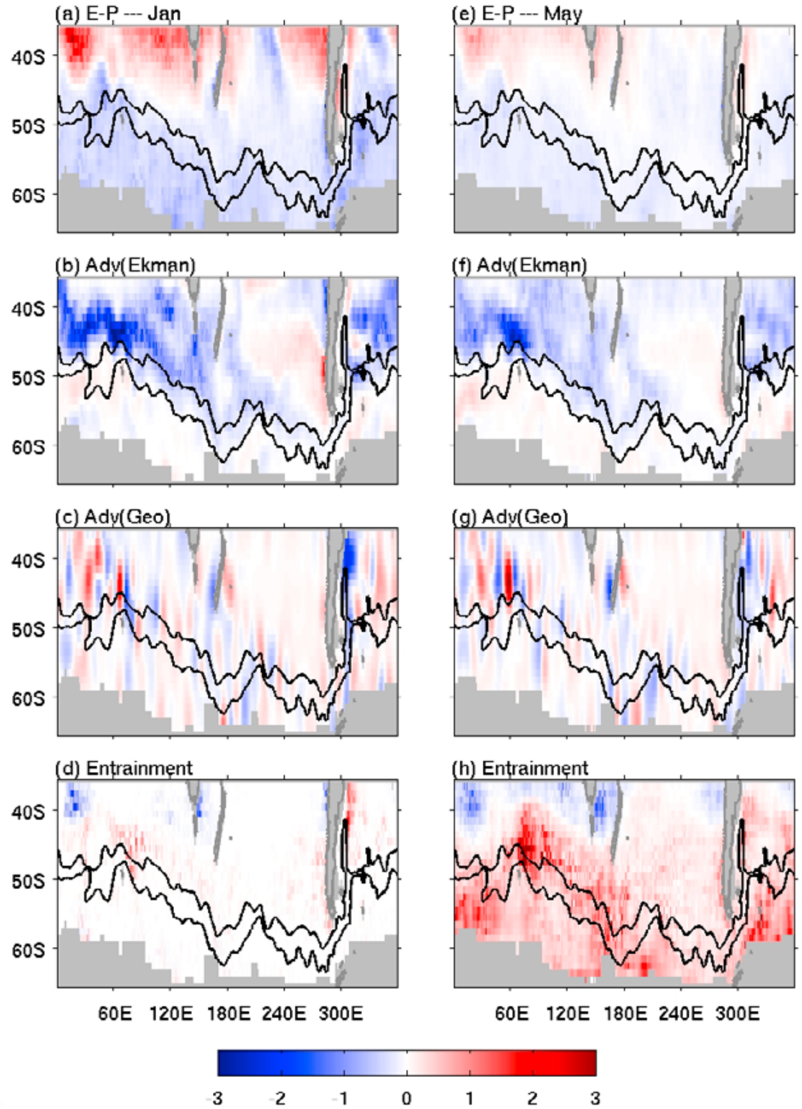

Figure 9. Spatial distribution of the atmospheric and oceanic processes in the salinity budget for (a–d) January and (e–h) May. Figures 9a and 9e denote the surface freshwater flux term (positive out of the ocean), Figures 9b and 9f denote Ekman advection, Figures 9c and 9g denote geostrophic advection, and Figures 9d and 9h denote vertical entrainment. Units are psu yr^{-1}.

the PF between 0 and 90°E. To the south of the SAF, the Ekman advection is weak due to both reduced wind and the weak gradient in the salinity field (Figure 6). In contrast to the large-scale spatial structure shown in the $E - P$ and Ekman advection terms, the geostrophic advection (Figure 9c) is dominated by small-scale features in the zonal direction, particularly along the ACC. A strong freshening effect of the geostrophic advection is seen in the Brazil-Falkland Confluence region (35°S–50°S, 300°E–330°E). The entrainment term (Figure 9d) is quite small in January and mostly positive. Relatively large values of entrainment are seen in the Brazil-Falkland Confluence region. In the northeast South Atlantic (35°S–40°S, 0–40°E), the entrainment shows negative values, suggesting that fresher subsurface water is entrained into the mixed layer. The diffusion term (not shown) is weak throughout the year, and its spatial distribution is very similar in each month.

[27] The salinity tendency in May (Figure 8d) shows a similar structure to that of January (Figure 8a), but with opposite sign. The salinity tendency is positive over most regions south of 45°S and is generally negative to the north. This indicates that the mixed layer becomes saltier in austral winter. Again, the sum of all of the contributions (Figure 8e) well captures the spatial distribution of the salinity tendency, although its magnitude is relatively large. The strong magnitude in the sum can be seen from the differences (Figure 8f) between the salinity tendency and the sum (Figure 8d minus Figure 8e), which show a similar structure as the sum, but with opposite sign. Both the $E - P$ term (Figure 9e) and Ekman advection (Figure 9f) show a similar structure to their counterparts in January, but their magnitudes in May are about half of those in January. In fact, the spatial structure of the $E - P$ and Ekman advection terms are similar year-round. The geostrophic advection (Figure 9g) also shows a similar structure to that in January (Figure 9c)

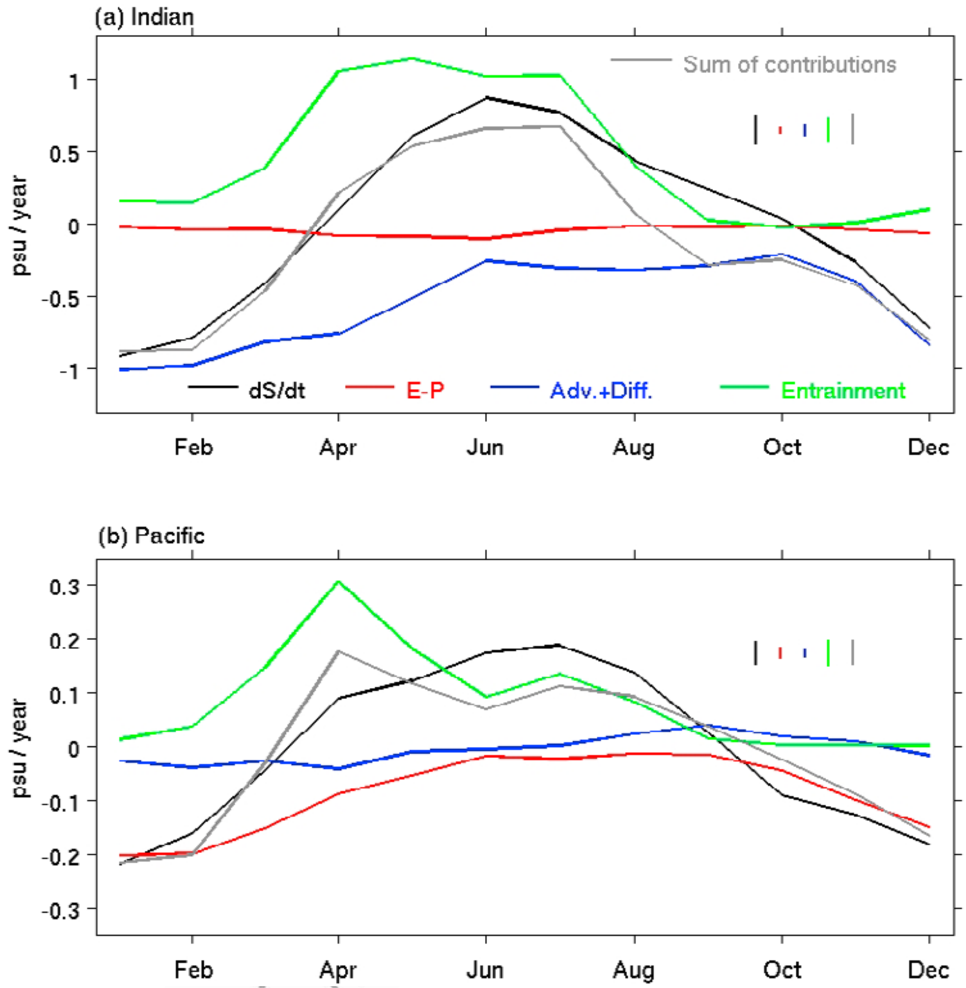

Figure 10. Salinity budget averaged over a 5° latitude band north of the SAF for (a) the Indian Ocean (80°E–120°E) and (b) the Pacific Ocean (240°E–280°E) where the deep mixed layer is formed in austral winter. The correspondence of the colors is the same as in Figure 5. The vertical lines correspond to one standard error for each term.

with comparable magnitude. The salinity increase in May is mainly due to the vertical entrainment process (Figure 9h), which is very strong and mostly positive south of 40°S. North of 40°S, except in the western part of the Pacific and Atlantic oceans, the entrainment shows negative values because the subsurface water entrained into the mixed layer is fresher when compared to the mixed layer water (Figure 4). The maximum entrainment appears in the Indian Ocean around the SAF (60°E–90°E).

3.2.3. Regional Budget

[28] As shown in Figure 1, salinity plays a larger role in the Indian Ocean than in the Pacific Ocean north of the SAF where the SAMW is formed. Thus, it is important to understand the differences in the salinity budget for these two regions, which will shed light on the regional similarities and differences of the mode water formation process. To examine the salinity balance in the Indian and Pacific oceans north of the SAF, we averaged the terms in equation (1) to a 5° latitude band to the north of the SAF, which corresponds to the regions with formation of the deep mixed layers. Figures 10a and 10b show the averaged terms in the two regions, respectively.

[29] The salinity budget in the Indian Ocean (Figure 10a) is similar to that averaged over the entire Southern Ocean (Figure 7). However, the magnitude of each term averaged in the Indian Ocean is three to four times larger, except for the $E - P$ term, which shows comparable magnitude with that averaged over the entire Southern Ocean. Similar to the domain average, the seasonal cycle of the salinity tendency is well captured by the sum of all of the contributions, with the exception being during August and September when the salinity tendency is positive, whereas the sum of the contributions produces negative values. The maximum and minimum salinity tendency occur in June and January, respectively. The $E - P$ term is very small and close to zero. The seasonal evolution of the mixed layer salinity is mainly controlled by the vertical entrainment and horizontal advection-diffusion processes. The entrainment term shows a strong seasonal cycle, but is always positive. The maximum entrainment occurs in April and May, one to two months prior to the peak of the salinity tendency. The advection-diffusion term, dominated by Ekman advection, is always negative, and its maximum freshening effect is in January. When combined with Figure 1, which shows that the

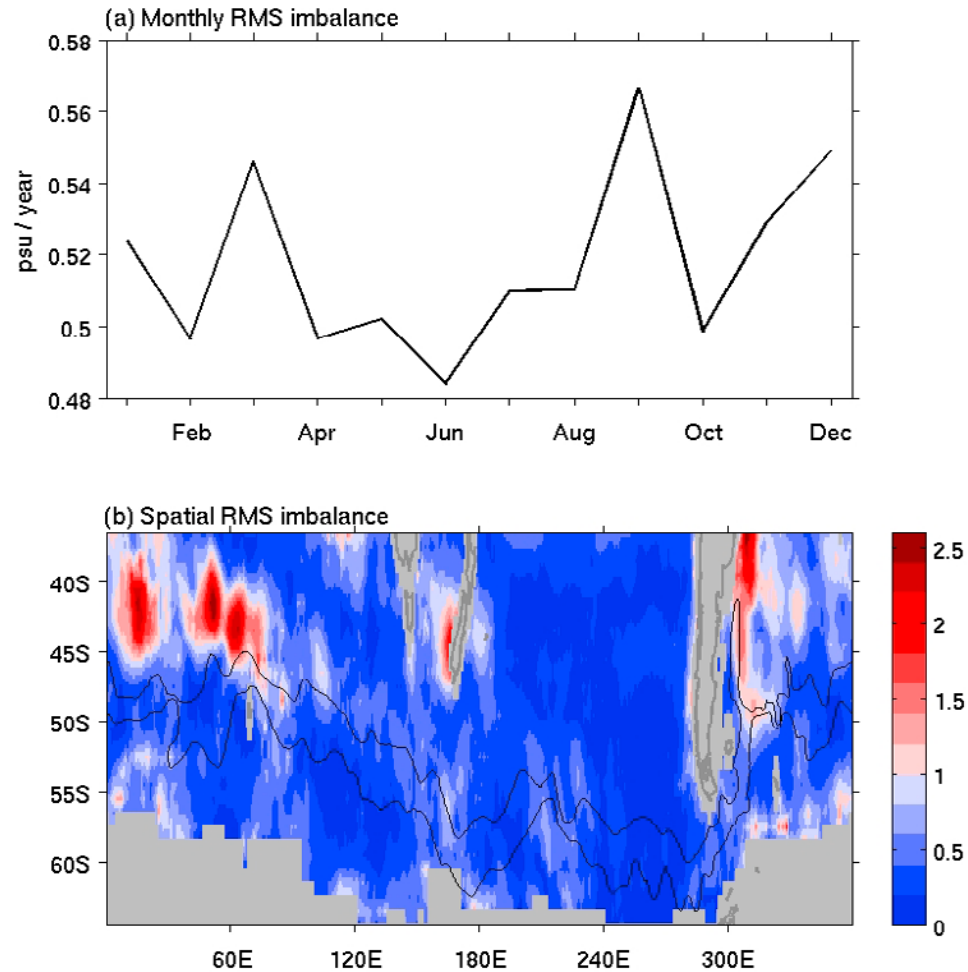

Figure 11. (a) Domain-averaged root-mean-square imbalance of the salinity budget. (b) Spatial distribution of the root-mean-square imbalance. Units are psu yr^{-1}.

salinity plays an equal or more important role in the density seasonal variation, this suggests that oceanic processes play an important role in the SAMW formation in the Indian Ocean on a seasonal time scale. In particular, vertical entrainment brings saltier water into the mixed layer from the subsurface and, subsequently, modifies the mixed layer density.

[30] The salinity budget in the Pacific Ocean north of the SAF (Figure 10b) shows a different scenario from that averaged over the entire Southern Ocean (Figure 7) and that in the Indian Ocean (Figure 10a). The magnitude and seasonal evolution of the salinity tendency are comparable with those averaged over the entire Southern Ocean. The salinity tendency reaches its maximum in July and minimum in January. The positive salinity tendency is due to the vertical entrainment term. In the Pacific, the $E - P$ term plays a dominant role in the freshening of the mixed layer, while the advection-diffusion term plays only a minimal role. The $E - P$ term is negative throughout the year with the maximum freshening effect in austral summer (January–February) and minimum in austral winter (June–September). The advection-diffusion is quite small and shows a weak seasonal cycle, with negative values in the austral summer and fall and positive values in the spring. An examination of the contributions from the geostrophic and Ekman components (not shown) suggests that the positive advection-diffusion comes from the meridional component of the geostrophic advection. Figure 1 shows that salinity plays a relatively small role in the density seasonal variation in the Pacific, suggesting that salinity may not be a primary driver of the SAMW formation in the South Pacific, at least on a seasonal time scale. Hence, even with its dominant role in the salinity seasonal changes, the importance of the $E - P$ in the formation of SAMW still needs further examination.

3.3. Imbalance

[31] If all the data were perfect, Figures 8a and 8b would be expected to be the same, as would be Figures 8d and 8e. Although the salinity tendency can be explained by the sum of all the terms in the domain average (Figure 7), large differences at individual locations appear in Figures 8c and 8f. We examined the imbalance (δ) in (1), defined as the difference between the salinity tendency (left-hand side in (1)) and the sum of all of the other terms (right-hand side in (1)), i.e., the difference between the black and gray lines in Figure 7. We first examined the domain-averaged imbalance (Figure 11a), the monthly root-mean-square (RMS) imbalance, $rms(\delta) = \sqrt{\sum \delta_i^2 / n}$, where δ_i is the imbalance at

each grid point *i*, and *n* is the number of data points for a given month. Figure 11a suggests that the RMS imbalance has no apparent seasonal variation, with an average rms(δ) of 0.52 psu yr^{-1}.

[32] To examine the spatial distribution of the imbalance, following the methodology for the monthly imbalance, we computed the RMS imbalance at each grid point. Here, δ_i is the imbalance at time *i*, and *n* is the number of data points at a given geographic location, which equals 12 in this case. In most regions, the RMS imbalance is less than 0.5 psu yr^{-1} (Figure 11b). A relatively large imbalance is seen around the SAF, whereas in the entire Pacific section the imbalance is small, close to zero, which is primarily due to the small values of the budget terms. One of the major features shown in Figure 11b is the large imbalance along the Brazil Current (35°S–50°S, 300°E–315°E) and in the broad Agulhas Retroflection region (40°S–45°S, 0–70°E). Both regions experience strong freshening (Figure 5c) from oceanic advection, which can be attributed to the strong salinity gradient (Figure 6) in these regions. This freshening from oceanic advection is only partially compensated by the positive $E - P$ term (Figure 5a), suggesting that the $E - P$ data may not fully capture the oceanic processes in these regions.

[33] Many factors can contribute to the imbalance, including errors in the constructed salinity fields, freshwater flux products, unaccounted for effects of seasonal ice melt or variations in river runoff, representation of the mixed layer depth, and velocity fields. Of these factors, the freshwater fluxes are expected to be the largest contributor to the mixed layer salinity budget error, as only limited Southern Hemisphere data are available for the reanalysis products and, hence, the reliability of these fluxes is uncertain. The regions near the sea ice edge do not experience a large RMS imbalance in the residual of the mixed layer salinity budget, which we take as confirmation that the effect of sea ice is not a dominant part of the residual. A detailed description of the sensitivity of the mixed layer salinity balance to the choice of data set is given in Appendix A. In summary, we found significant differences in the RMS imbalance if we change our choice of $E - P$, mixed layer depth, and salinity field. Changing the choice of wind product and mean geostrophic velocity does not have a significant influence on the results. This suggests that a better mixed layer salinity budget for the Southern Ocean can be achieved by improving the accuracy of the freshwater flux products, increasing the spatial sampling of the salinity field, particularly in regions with strong eddy activity, and improving the representation of the mixed layer depth.

4. Discussion and Conclusions

[34] In this study, the seasonal mixed layer salinity balance in the Southern Ocean (0–360°E, 35°S–65°S) was examined from a combination of remotely sensed and in situ observations. An examination of the time-mean balance indicated that, although the spatial structure of the freshwater flux term is similar to that of the oceanic processes (advection, diffusion, and entrainment) with opposite sign as expected, its magnitude is relatively small, consistent with the results for the tropics [*Johnson et al.*, 2002].

[35] For the domain average, the mixed layer salinity undergoes a seasonal cycle. It increases from March to October and decreases from November to February. This seasonal evolution in salinity is well captured by the sum of the contributions from the oceanic and atmospheric processes. However, the sum of the contributions shows a negative bias. Unlike the mixed layer temperature budget in the Southern Ocean where the air-sea heat fluxes dominate the temperature seasonal cycle, freshwater fluxes play a minimal role in the salinity seasonal cycle. The seasonal variation in the mixed layer salinity is dominated by vertical entrainment, which can be mostly attributed (above 70%) to the seasonality of the vertical entrainment velocity. The advection-diffusion term, dominated by meridional Ekman advection, plays a secondary role.

[36] The sum of all of the contributions also captures the spatial structure of the salinity tendency. South of 40°S, the salinity tendency is spatially coherent; it increases from March to October and decreases from November to February. To the north of 40°S, the seasonal variation in salinity tendency is generally opposite to that south of 40°S. The spatial structure of each term is similar throughout the year, although its magnitude changes with time. The freshwater flux term is negative south of 45°S and positive to the north. The Ekman advection acts to decrease salinity in most regions with the maximum freshening effect just to the north of the SAF. The geostrophic advection is dominated by relatively small-scale structures, particularly near the vicinity of the ACC. The entrainment is mostly positive except near the northern boundary, suggesting that more saline water is entrained into the mixed layer from the subsurface.

[37] Although both the seasonal evolution and spatial structure of the mixed layer salinity are fairly captured by the atmospheric and oceanic processes, substantial imbalances exist in the regional salinity budget. On average, the mixed layer salinity budget in the Southern Ocean has a root-mean-square imbalance of 0.52 psu yr^{-1}. Large discrepancies between the salinity tendency and the sum of the contributions from the air-sea freshwater flux, advection, diffusion, and entrainment terms are found in the Brazil-Falkland Confluence and Agulhas Retroflection regions. These regions collocate with regions of the highest kinetic energy in the Southern Ocean (Figure 12), suggesting that the eddy dynamics in these high energetic regions may not be well represented in existing data products, specifically for the freshwater flux products and the salinity fields from in situ measurements whose spatial distribution tends to be biased. An examination of the spatial distribution of the Argo float profiles (Figure 3a) shows that the profiles in regions with a strong RMS imbalance are relatively sparse. Thus, the spatial structure of the salinity field may not be well captured by salinity objective maps, suggesting that an increase in the salinity measurements in these energetic regions can potentially improve the salinity budget.

[38] Various sensitivity tests were performed to evaluate the contributions of uncertainties in different data sets to the imbalance. No significant differences in the RMS imbalance were found using different mean geostrophic advection or

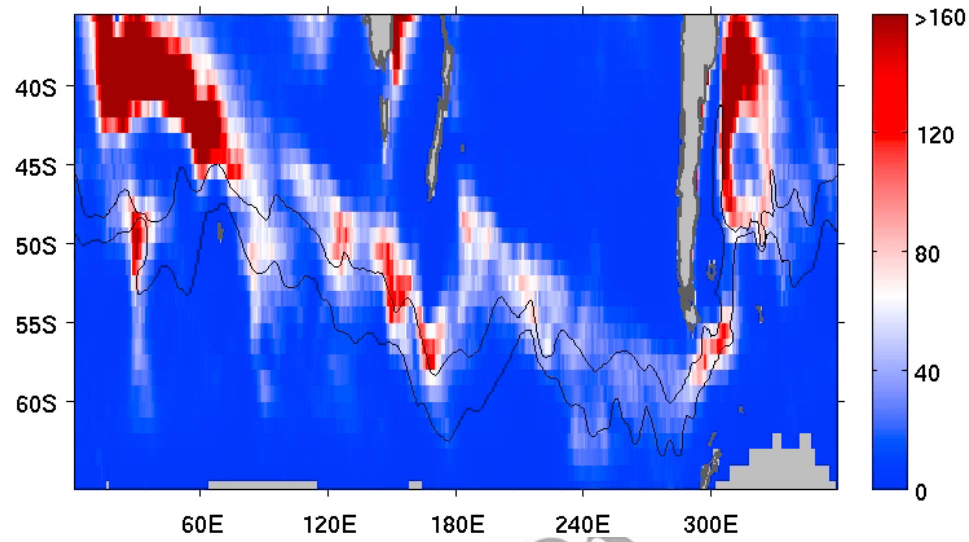

Figure 12. The temporally averaged (1993–2007) eddy kinetic energy (EKE) derived from AVISO geostrophic velocity data [(EKE = $(u'^2 + v'^2)/2$]. Units are cm^2 s^{-2}.

wind stress fields. This indicates that the uncertainties in the velocity fields are not the major contributors to the imbalance. Results from six different net freshwater fluxes (see Appendix A for detail) showed significant differences in the RMS imbalance, suggesting that a better freshwater flux product is needed to close the budget. Significant differences in the RMS imbalance were also found when the salinity climatology from the World Ocean Atlas 2005 (WOA05) was used. Using the WOA05 salinity product instead of those derived from Argo profiles gave a RMS imbalance of 0.88 psu yr^{-1}. This large difference is probably due to the lack of salinity measurements in the WOA05 for the Southern Ocean since 70% of the Argo float profiles used in our salinity maps were collected after 2005. This suggests that a better salinity field is important to close the budget. Hence, it is critical to accumulate salinity measurements continuously.

[39] The Aquarius satellite, which is planned for launch in 2010, will provide monthly maps of global surface salinity with an accuracy of 0.2 psu. The Argo profiles show that the surface salinity and mixed layer salinity differ by only 0.001 psu on average with a standard deviation of 0.01 psu, suggesting that satellite observations of surface salinity well represent the mixed layer salinity, at least in the Southern Ocean. To examine the accuracy of the surface salinity measurements required to provide a better salinity budget, we applied a Monte Carlo technique where random errors with RMS(S) were added to the salinity maps. We then examined the RMS differences between the salinity tendency ($\partial S/\partial t$) from the original maps (considered as 'truth') and that from the salinity maps with random errors. This process was repeated with different magnitudes of salinity error, i.e., by varying the RMS(S) from 0 to 0.5 psu. Our examination suggested that, to achieve results that are better than the uncertainties (~0.52 psu yr^{-1}) induced by freshwater flux and oceanic processes for the Southern Ocean, satellite salinity measurements need to have an accuracy of 0.12 psu or less. Nevertheless, the spatial resolution of the salinity measurements from space, particularly for regions with strong eddy activity, has the potential to provide a better representation of the spatial salinity gradients and, hence, provide better estimates of the oceanic advection and diffusion processes.

Appendix A: Sensitivity of the Salinity Budget to Choice of Data

[40] The results of the mixed layer salinity budget in the Southern Ocean presented in sections 3.1 and 3.2 are our best estimate from existing data with S_m, h_m, and ΔS from Argo float profiles; freshwater flux from ECMWF; geostrophic velocity from AVISO; and Ekman velocity from COAPS winds. These data form our "base case" estimate of the mixed layer salinity budget. The base case has a rms(δ) of 0.52 ± 0.03 psu yr^{-1}, where the error bars are twice the standard error. To help evaluate how the uncertainties in these data influence the mixed layer salinity budget on a seasonal time scale, we examined the sensitivity of the salinity budget to the choice of data set.

[41] Various data sets were used in the sensitivity test, including mean geostrophic velocity data derived from the mean SSH of *Maximenko and Niiler* [2005] and GRACE [*Tapley et al.*, 2003]; Ekman velocity-derived data from the surface wind stress fields of the National Center for Environmental Prediction/National Center for Atmospheric Research (NCEP/NCAR) reanalysis and that from a blended sea wind product from the National Climate Data Center [*Zhang et al.*, 2006]; a mixed layer depth climatology from *de Boyer Montegut et al.* [2004], World Ocean Atlas 1994 (WOA94), and the World Ocean Atlas 2001 (WOA01). No significant differences in the RMS imbalance were found using various geostrophic and Ekman velocity fields. Similar to the heat budget in the Southern Ocean [*Dong et al.*, 2007], the RMS imbalances of the salinity budget based on different mixed layer depth products are significantly different, with a maximum rms(δ) of 0.93 ± 0.06 psu yr^{-1} using h_m from WOA94. This suggests that a proper repre-

sentation of the mixed layer depth is important to close the budget.

[42] Six net freshwater flux ($E - P$) climatologies, including the ECMWF reanalysis 40, were tested. In addition to the monthly climatology from the NCEP/NCAR reanalysis [*Kalnay et al.*, 1996] and that from the Southampton Oceanography Centre (SOC) [*Josey et al.*, 1998], three blended climatologies were constructed using evaporation (E) data from the OAFlux and precipitation (P) data from the Climate Prediction Center Merged Analysis of Precipitation (CMAP), enhanced CMAP (CMPAE) [*Xie and Arkin*, 1997], and Global Precipitation Climatology Project (GPCP) [*Adler et al.*, 2003], i.e., E(OAFlux) $-$ P(CMAP), E(OAFlux) $-$ P(CMAPE), and E(OAFlux) $-$ P(GPCP). Both the CMAP and GPCP precipitation were developed using multisatellite estimates only, whereas the CMAPE precipitation also included precipitation values from the NCEP/NCAR reanalysis. All three satellite-based precipitation products are available from 1979 to the present on a monthly basis with a spatial resolution of 2.5° of latitude and longitude. To be consistent with the Argo and OAFlux time periods, the three blended $E - P$ climatologies were constructed from averages between 2000 and 2006. The SOC flux climatology, with a spatial resolution of $1^\circ \times 1^\circ$, was derived from in situ meteorological reports in the Comprehensive Ocean Atmosphere Data set 1a (COADS) covering the period 1980–1993. Of the six net freshwater flux products, the ECMWF gave the smallest RMS imbalance (0.52 ± 0.03 psu yr^{-1}) and the SOC flux the largest RMS imbalance of 0.65 ± 0.04 psu yr^{-1}. The differences in the RMS imbalance from the various $E - P$ products suggest that a better freshwater flux product is needed to advance the understanding of salinity variability and the processes controlling it.

[43] Ekman advection may be sensitive to assumptions about the Ekman depth, i.e., the depth of penetration of the wind-driven flow. In this study, we used the mixed layer depth, h_m, as the Ekman depth. In cases where the true Ekman depth is shallower than h_m, the Ekman advection is confined to the mixed layer, and the Ekman depth does not influence the salinity budget. However, if the Ekman depth is deeper than h_m, the Ekman velocities are overestimated, resulting in an overestimate of the Ekman advection in the mixed layer. To test the sensitivity of the mixed layer salinity budget to a deeper Ekman depth, we increased the Ekman depth to twice that of h_m, which effectively reduced the Ekman transport within the mixed layer to one half of its original value. The RMS imbalance decreased by 0.04 psu yr^{-1}. Another test we performed was to assume that the Ekman depth is no less than 100 m, i.e., the Ekman depth is set to be 100 m whenever h_m is shallower than 100 m. The RMS imbalance was reduced by 0.03 psu yr^{-1}. These tests suggest that a better knowledge of the Ekman depth can improve the mixed layer salinity budget in the Southern Ocean.

[44] Unlike the mixed layer temperature whose variations in space and time can be well represented by satellite SST measurements with continuous spatial and temporal coverage, existing salinity maps are derived from sparse in situ measurements. The uncertainties in the salinity field may contribute to the imbalance. We examined the sensitivity of the salinity budget to S_m by making use of the salinity climatology from the World Ocean Atlas 2005 (WOA05). With all of the other data sets the same as our base case, the results using S_m from the WOA05 gave an average RMS imbalance of 0.88 ± 0.06 psu yr^{-1}. The large difference from our base case is probably due to the lack of salinity data in the World Ocean Database 2005, as the majority of the Argo profiles (70%) were from the post-2005 period. Although the spatial structure of the salinity data from the WOA05 is similar to our objective map for the Argo float profiles, the WOA05 field is much smoother, particularly around the ACC where the salinity gradient is the largest. This suggests that it is important to continuously accumulate salinity measurements with better spatial resolution to resolve the relatively fine structure of the salinity field. Ultimately, an improved salinity field for the Southern Ocean will improve our understanding of the upper ocean processes governing the meridional overturning circulation.

[45] Note that the residual imbalance included some unresolved variations due to seasonal changes in the freshwater fluxes from sea ice. To further quantify the effect of sea ice seasonal variations, we used the monthly sea ice area from the National Snow and Ice Data Center of the University of Colorado, which suggested a total Antarctic ice area change of $\sim 12 \times 10^{12}$ m^2 on a seasonal time scale. This gave a freshwater input/output of 12×10^{12} m^3 assuming a sea ice thickness of 1 m (typical for the Antarctic sea ice). If we assume this amount of freshwater is evenly distributed in our study region, it is equivalent to 0.13 m yr^{-1} freshwater input/output, which is about 20% of the RMS difference between the freshwater fluxes from SOC and ECMWF. Thus, the seasonal variations in sea ice is not a large contributor to the salinity imbalance when compared to the uncertainties in the $E - P$ data.

[46] **Acknowledgments.** The authors thank Carlisle Thacker and the two anonymous reviewers for their helpful comments. The authors also thank Gail Derr for her grammatical corrections. The Argo float profiles are managed by the Global Ocean Data Assimilation Experiment and are available at http://www.usgodae.org/ftp/outgoing/argo/dac/. The altimeter SSH anomalies were produced by Ssalto/Duacs and are distributed by AVISO with support from the Centre National d'Etudes Spatiales. The NCEP reanalysis-derived data were provided by the Physical Sciences Division of NOAA's Earth System Research Laboratory in Boulder, Colorado, USA, from their web site at http://www.esrl.noaa.gov/psd/. The pseudostress fields were produced at COAPS and are available at http://www.coaps.fsu.edu/scatterometry/Qscat/.

References

Adler, R. F., et al. (2003), The version-2 Global Precipitation Climatology Project (GPCP) monthly precipitation analysis (1979–present), *J. Hydrometeorol.*, *4*(6), 1147–1167, doi:10.1175/1525-7541(2003)004<1147:TVGPCP>2.0.CO;2.

Antonov, J. I., S. Levitus, and T. P. Boyer (2002), Steric sea level variations during 1957–1994: Importance of salinity, *J. Geophys. Res.*, *107*(C12), 8013, doi:10.1029/2001JC000964.

Boyer, T. P., S. Levitus, J. I. Antonov, R. A. Locarnini, and H. E. Garcia (2005), Linear trends in salinity for the World Ocean, 1955–1998, *Geophys. Res. Lett.*, *32*, L01604, doi:10.1029/2004GL021791.

Cronin, M. F., and M. J. McPhaden (1998), Upper ocean salinity balance in the western equatorial Pacific, *J. Geophys. Res.*, *103*, 27,567–27,588, doi:10.1029/98JC02605.

Curry, R., B. Dickson, and I. Yashayaev (2003), A change in the freshwater balance of the Atlantic Ocean over the past four decades, *Nature*, *426*, 826–829, doi:10.1038/nature02206.

de Boyer Montegut, C., G. Macde, A. S. Fischer, A. Lazar, and D. Iudicone (2004), Mixed layer depth over the global ocean: An examination of profile data and a profile-based climatology, *J. Geophys. Res.*, *109*, C12003, doi:10.1029/2004JC002378.

de Boyer Montegut, C., J. Mignot, A. Lazar, and S. Cravatte (2007), Control of salinity on the mixed layer depth in the world ocean: 1. General description, *J. Geophys. Res.*, *112*, C06011, doi:10.1029/2006JC003953.

Dong, S., and K. A. Kelly (2004), Heat budget in the Gulf Stream region: The importance of heat storage and advection, *J. Phys. Oceanogr.*, *34*, 1214–1231, doi:10.1175/1520-0485(2004)034<1214:HBITGS>2.0.CO;2.

Dong, S., S. T. Gille, and J. Sprintall (2007), An assessment of the Southern Ocean mixed-layer heat budget, *J. Clim.*, *20*, 4425–4442, doi:10.1175/JCLI4259.1.

Dong, S., J. Sprintall, S. T. Gille, and L. Talley (2008), Southern Ocean mixed depth from Argo float profiles, *J. Geophys. Res.*, *113*, C06013, doi:10.1029/2006JC004051.

Ducet, N., P.-Y. Le Traon, and G. Reverdin (2000), Global high resolution mapping of ocean circulation from TOPEX/POSEIDON and ERS-1 and -2, *J. Geophys. Res.*, *105*, 19,477–19,498, doi:10.1029/2000JC900063.

Foltz, G. R., and M. J. McPhaden (2008), Seasonal mixed layer salinity balance of the tropical North Atlantic Ocean, *J. Geophys. Res.*, *113*, C02013, doi:10.1029/2007JC004178.

Foltz, G. R., S. A. Grodsky, J. A. Carton, and M. J. McPhaden (2004), Seasonal salt budget of the northwestern tropical Atlantic Ocean along 38°W, *J. Geophys. Res.*, *109*, C03052, doi:10.1029/2003JC002111.

Gould, J. and the Argo Steering Team (2004), Argo profiling floats bring new era of in situ ocean observations, *Eos Trans. AGU*, *85*(19), doi:10.1029/2004EO190002.

Johnson, E. S., S. E. Lagerloef, J. T. Gunn, and F. Bonjean (2002), Surface salinity advection in the tropical oceans compared with atmospheric freshwater forcing: A trial balance, *J. Geophys. Res.*, *107*(C12), 8014, doi:10.1029/2001JC001122.

Josey, S. A., E. C. Kent, and P. K. Taylor (1998), The Southampton Oceanography Centre (SOC) ocean-atmosphere heat, momentum, and freshwater flux atlas, *Rep. 6*, 59 pp., Southampton Oceanogr. Cent., Southampton, U. K.

Kalnay, E., et al. (1996), The NCEP/NCAR 40-year reanalysis project, *Bull. Am. Meteorol. Soc.*, *77*, 437–471, doi:10.1175/1520-0477(1996)077<0437:TNYRP>2.0.CO;2.

Maes, C. (1998), Estimating the influence of salinity on sea level anomaly in the ocean, *Geophys. Res. Lett.*, *25*(19), 3551–3554, doi:10.1029/98GL02758.

Maes, C., M. J. McPhaden, and D. Behringer (2002), Signatures of salinity variability in tropical Pacific Ocean dynamic height anomalies, *J. Geophys. Res.*, *107*(C12), 8012, doi:10.1029/2000JC000737.

Maximenko, N. A., and P. P. Niiler (2005), Hybrid decade-mean global sea level with mesoscale resolution, in *Recent Advances in Marine Science and Technology, 2004*, edited by N. Saxena, pp. 55–59, PACON Int., Honolulu.

Pegion, P. J., M. A. Bourassa, D. M. Legler, and J. J. O'Brien (2000), Objectively derived daily "winds" from satellite scatterometer data, *Mon. Weather Rev.*, *128*, 3150–3168, doi:10.1175/1520-0493(2000)128<3150:ODDWFS>2.0.CO;2.

Qiu, B., and K. A. Kelly (1993), Upper-ocean heat balance in the Kuroshio Extension region, *J. Phys. Oceanogr.*, *23*, 2027–2041, doi:10.1175/1520-0485(1993)023<2027:UOHBIT>2.0.CO;2.

Rintoul, S. R., and M. H. England (2002), Ekman transport dominates local air-sea fluxes in driving variability of Subantarctic Mode Water, *J. Phys. Oceanogr.*, *32*, 1308–1321, doi:10.1175/1520-0485(2002)032<1308:ETDLAS>2.0.CO;2.

Roemmich, D. (1983), Optimal estimation of hydrographic station data and derived fields, *J. Phys. Oceanogr.*, *13*, 1544–1549, doi:10.1175/1520-0485(1983)013<1544:OEOHSD>2.0.CO;2.

Roemmich, D., J. Gilson, J. Willis, P. Sutton, and K. Ridgway (2005), Closing the time-varying mass and heat budgets for large ocean areas: The Tasman Box, *J. Clim.*, *18*, 2330–2343, doi:10.1175/JCLI3409.1.

Sloyan, B., and S. R. Rintoul (2001), Circulation, renewal and modification of Antarctic mode water and intermediate water, *J. Phys. Oceanogr.*, *31*, 1005–1030, doi:10.1175/1520-0485(2001)031<1005:CRAMOA>2.0.CO;2.

Tapley, B. D., D. P. Chambers, S. Bettadpur, and J. C. Ries (2003), Large scale ocean circulation from the GRACE GGM01 Geoid, *Geophys. Res. Lett.*, *30*(22), 2163, doi:10.1029/2003GL018622.

Uppala, S. M., et al. (2005), The ERA-40 reanalysis, *Q. J. R. Meteorol. Soc.*, *131*, 2961–3012, doi:10.1256/qj.04.176.

Vivier, F., K. A. Kelly, and L. Thompson (2002), Heat budget in the Kuroshio Extension region: 1993–1999, *J. Phys. Oceanogr.*, *32*, 3436–3454, doi:10.1175/1520-0485(2002)032<3436:HBITKE>2.0.CO;2.

Wong, A. P. S., N. L. Bindoff, and J. A. Church (1999), Large-scale freshening of intermediate waters in the Pacific and Indian oceans, *Nature*, *400*, 440–443, doi:10.1038/22733.

Xie, P., and P. A. Arkin (1997), Global precipitation: A 17-year monthly analysis based on gauge observations, satellite estimates, and numerical model outputs, *Bull. Am. Meteorol. Soc.*, *78*, 2539–2558, doi:10.1175/1520-0477(1997)078<2539:GPAYMA>2.0.CO;2.

Yelland, M., and P. K. Taylor (1996), Wind stress measurements from the open ocean, *J. Phys. Oceanogr.*, *26*, 541–558, doi:10.1175/1520-0485(1996)026<0541:WSMFTO>2.0.CO;2.

Yu, L., and R. A. Weller (2007), Objectively Analyzed air-sea heat Fluxes (OAFlux) for the global oceans, *Bull. Am. Meteorol. Soc.*, *88*, 527–539, doi:10.1175/BAMS-88-4-527.

Zhang, Y.-C., W. B. Rossow, A. A. Lacis, V. Oinas, and M. I. Mishchenko (2004), Calculation of radiative fluxes from the surface to top of atmosphere based on ISCCP and other global data sets: Refinements of the radiative transfer model and the input data, *J. Geophys. Res.*, *109*, D19105, doi:10.1029/2003JD004457.

Zhang, H.-M., J. J. Bates, and R. W. Reynolds (2006), Assessment of composite global sampling: Sea surface wind speed, *Geophys. Res. Lett.*, *33*, L17714, doi:10.1029/2006GL027086.

M. Baringer and S. L. Garzoli, NOAA, AOML, 4301 Rickenbacker Causeway Miami, FL 33149, USA.

S. Dong, CIMAS, RSMAS, University of Miami, 4301 Rickenbacker Causeway, Miami, FL 33149, USA. (shenfu.dong@noaa.gov)